

Pushing the Envelope of LLM Inference on AI-PC and Intel GPUs

Evangelos Georganas, Dhiraj Kalamkar, Alexander Heinecke
Intel Corporation

Abstract—The advent of ultra-low-bit LLM models (1/1.58/2-bit), which match the perplexity and end-task performance of their full-precision counterparts using the same model size, is ushering in a new era of LLM inference for resource-constrained environments such as edge devices and AI PCs. While these quantization advances promise models that are more cost-effective in terms of latency, memory, throughput, and energy consumption, the computational efficiency of state-of-the-art (SOTA) inference runtimes (e.g., bitnet.cpp) used to deploy them remains underexplored. In this work, we take a bottom-up approach: we first design and implement 1-bit and 2-bit microkernels optimized for modern CPUs, achieving peak computational efficiency across a variety of CPU platforms. We integrate these microkernels into a state-of-the-art LLM inference framework, namely PyTorch-TPP, and present end-to-end inference results with 2-bit models that outperform the current SOTA runtime bitnet.cpp by up to 2.2 \times , and deliver up to 7 \times speedup compared to the 16-bit model inference. We then extend this work to Intel GPUs where we design and implement mixed precision, 2-bit GEMM kernels, and show their performance to be close to optimal. We integrated our optimized Xe2 kernels in the vLLM framework as a quantization plugin and evaluated end-to-end LLM inference results for a range of LLM models and Xe2 GPUs. Depending on the model and platform, we see a 4 \times - 8 \times reduction in GEMM time compared to the BF16 case, and we get up to 6.3 \times speedup in end-to-end latency compared to the BF16 execution. Our optimized runtime advances the state of LLM inference on AI PCs and Intel Xe GPUs, paving the way for efficient deployment of ultra-low-bit LLM models.

I. INTRODUCTION

Recent advances in Quantization-Aware Training (QAT) LLM methods have produced ultra-low bit (1-bit, 1.58-bit and 2-bit) quantized models that match the perplexity and end-task performance of their full-precision counterparts using the same model size [1], [2]. Despite these advancements that yield ultra-low bit LLM models with the *potential* to be cost-effective in terms of latency, memory, throughput, and energy consumption, the available runtimes capable of serving inference with such models are limited. For example, the state-of-the-art inference runtime bitnet.cpp is specifically designed for ternary LLMs, with a relatively narrow range of applicable model architectures [3]. Additionally, although the bitnet.cpp runtime improves upon alternatives (e.g. llama.cpp) being up to 6 \times faster by introducing a specialized mixed-precision matrix multiplication (mpGEMM) library to facilitate sub-2-bits model inference, its efficiency is not evaluated in terms of optimality or roofline performance. Our preliminary performance analysis showed that 2-bit inference with bitnet.cpp was even *slower* than state-of-the-art 4-bit inference on CPUs (e.g.

see in Figures 13, 12, 14 the orange and the magenta bars), highlighting that the bitnet.cpp runtime is far from optimal.

In this work we adopt a bottom-up approach to address the performance shortcomings of bitnet.cpp. The key observation is that client/edge inference typically involves single-batch use-cases, which in turn result in memory-bound matrix multiplication invocations (more precisely matrix-vector multiplication) during the execution. By exploiting the reduced bit-width of the model’s weight tensors during inference we can accelerate the corresponding matrix-vector multiplications (e.g. compared to the case with 16-bit weight tensors), since the volume of data read on the critical path is proportional to the bit-width of the weight datatype. First, we designed and implemented 1-bit and 2-bit mixed-precision matrix multiplication (GEMM) routines that up-convert the low-precision weight matrices (1- or 2-bit entries) to 8-bit integers, and perform the fused-multiply-add (FMA) operations using hardware-accelerated instructions on modern CPUs. We introduce novel weight layouts that facilitate the up-convert process, and within the GEMM microkernels we deploy instruction sequences that maximize the throughput of the “up-convert and compute” steps. We also construct performance models for the introduced kernels to assess their efficacy and show that they achieve close to peak roofline performance on modern CPU platforms. Furthermore, we compose these microkernels into optimized multi-threaded GEMM routines that leverage dynamic task scheduling to fully exploit the heterogeneous architectures with *performance* and *efficiency* cores. We benchmark these multi-threaded GEMM routines on a variety of modern x86 CPU platforms. Finally, we integrate these ultra-low bit GEMM routines in a SOTA inference framework, namely PyTorch TPP [4], and showcase end-to-end inference results using 2-bit and 1-bit models. Our optimized 2-bit inference is up to 7 \times faster than the 16-bit inference, and outperforms bitnet.cpp by up to 2.2 \times .

Then we extend this work to Intel Xe2 GPUs where we design and implement mixed precision, 2-bit GEMM kernels. While contemporary Xe2 Intel GPUs support natively $\text{int2}\times\text{int8}\rightarrow\text{int32}$ GEMM computations using hardware acceleration, the SOTA ultra-low bit inference (e.g. 2-bit weights) requires high-precision (e.g. BF16) input/output activations, i.e. $\text{int2}\times\text{BF16}\rightarrow\text{BF16}$ GEMM. Quantizing the input activations from BF16 to int8 *before* the $\text{int2}\times\text{int8}\rightarrow\text{int32}$ GEMM operation, and dequantizing the int32 GEMM output to BF16 output activations via separate microkernels out of L1/L2 cache adds minimal overhead for the CPU use-case.

However, on GPUs such a decoupled execution of activation-quantization \rightarrow low-precision GEMM microkernel \rightarrow output-dequantization incurs multiple kernel launches and passes over the data. Therefore, we developed mixed precision $\text{int}2 \times \text{BF}16 \rightarrow \text{BF}16$ GEMM Xe2 kernels that fuse the input/output activation quantization/dequantization within the GEMM kernel to minimize the corresponding overheads. We integrated our optimized Xe2 kernels in the vLLM [5] framework as a quantization plugin and evaluated end-to-end LLM inference results for a range of LLM models and Intel Xe2 GPUs. Depending on the model and platform, we see a $4 \times - 8 \times$ reduction in GEMM time compared to the BF16 case, and we get up to $6.3 \times$ speedup in end-to-end latency compared to the BF16 execution.

The contributions of this work are:

- We designed and implemented 1-bit and 2-bit GEMM kernels tailored for CPUs with AVX2 ISA. These kernels leverage novel blocked and interleaved weight tensor layouts to facilitate the up-convert process during inference. We devised performance models that characterize the effectiveness and limitations of these kernels. We composed these new CPU microkernels into multi-threaded GEMM routines targeting hybrid-core architectures. Also, we benchmarked the new routines on a set of matrices and platforms, showing that they can achieve the attainable memory bandwidth, effectively accelerating the bandwidth-bound matrix-vector multiplication operations proportionally to the bit-width of the weight’s datatypes.
- We designed and implemented mixed precision GEMM kernels targeting Intel GPUs with Xe2 cores. These kernels fuse the quantization/dequantization of the input/output activations and leverage the hardware accelerated $\text{int}2 \times \text{int}8$ Dot Product Accumulate Systolic (DPAS) instructions. We benchmarked the mixed precision GEMM kernels under different scenarios and show they can achieve bandwidth close to the platform’s limit, accelerating matrix-vector multiplication operations proportionally to the bit-width of the weight’s datatypes. We also achieve compute throughput close to the ideal $\text{int}2 \times \text{int}8$ DPAS throughput, highlighting the efficacy of our fused quantization/dequantization, and these Xe2 GEMM kernels can be further used to accelerate compute-bound use-cases in LLM inference (e.g. prefill phase, larger batch-size inference).
- We integrated these ultra-low bit GEMM kernels in SOTA end-to-end inference pipelines (PyTorch-TTP for CPU, vLLM for GPU), assessed their performance on a range of models and platforms, and observed speedups up to $7 \times$ over the 16-bit inference. We benchmarked our runtime against bitnet.cpp and show that our proposed solution is up to $2.2 \times$ faster.
- We compare our CPU performance with the optimized GPU 2-bit inference within bitnet.cpp, which includes kernels specifically tailored for the NVIDIA A100 platform. Our performance on contemporary x86 AI-PC

CPUs is within $2.3 \times - 3 \times$ of the A100 GPU, which has $17 \times - 20 \times$ more bandwidth than the CPU platforms. On a discrete Intel Arc B580 Xe2 GPU we achieve a speedup of $1.5 \times$ over the 2-bit inference on A100 for a same-sized 2 Billion parameter model, despite A100 having $4 \times$ more bandwidth than B580. Thus, our work pushes the envelope of LLM inference on AI-PCs and Intel Xe GPUs, and demonstrates that ultra-low-bit inference even on CPUs and discrete client GPUs can approach high-end GPU-level performance.

II. RELATED WORK

A. LLM Inference and ultra-low bit Quantization

In recent years, several methods have been developed by academia and industry to reduce LLM inference costs [6], minimize latency and increase efficiency, including sparsification/pruning [7], knowledge distillation [8], [9] and quantization [10]–[12]. Among these, quantization reduces the precision of model weights (e.g. from 16-bits to 4-bits/2-bits/1-bit), thereby lowering memory requirements and potentially accelerating inference, especially when the target hardware supports specialized instructions or when the pipeline operates in a bandwidth-bound regime [13]. Quantization methods for LLMs generally fall into two categories: Quantization-Aware Training (QAT) and Post-Training Quantization (PTQ). QAT incorporates reduced-precision weights directly into the model’s pretraining or fine-tuning process. By accounting for quantization effects during training, QAT enables the model to adjust its parameters with awareness of limited precision, resulting in better accuracy during quantized inference. In contrast, PTQ applies quantization to a pretrained model without additional training or fine-tuning. Although QAT typically achieves higher accuracy, it is more computationally intensive and requires access to representative training datasets [2].

As LLMs continue to scale in size and training data, increasing attention has been drawn to scaling laws that balance model size and dataset size to optimize performance and computational efficiency [14]–[16]. In parallel, the field is moving towards ultra-low-bit LLMs, motivated by the significant gains in memory and compute efficiency [1], [2], [17]. This trend calls for a re-evaluation of scaling laws to consider the impact of quantization on model performance. Recent work shows that 1.58-bit (ternary) and 2-bit quantization deliver performance comparable to full-precision models in the size–accuracy trade-off, and generally outperform both 4-bit and binary quantization [2].

B. Accelerating ultra-low-bit LLM Inference

Despite the promising results of ultra-low-bit LLMs, practical inference on edge devices remains a challenge. Recent work, such as Bitnet.cpp [3], introduced an inference engine tailored for BitNet b1.58b [1] and ternary LLMs. Bitnet.cpp includes a custom GEMM library designed for efficient, lossless inference with sub 2-bits per weight. While Bitnet.cpp improves upon existing frameworks like llama.cpp [18]

(achieving up to $6\times$ speedup thanks to a specialized mixed-precision matrix multiplication kernel), its efficiency has not been assessed in terms of optimality or roofline performance. Our preliminary analysis found that 2-bit inference with `Bitnet.cpp` was *slower* than state-of-the-art 4-bit inference on CPUs with PyTorch-TPP [19]. Prior research has explored primarily lookup-table (LUT)-based mixed-precision GEMMs in deep learning [20]–[23], especially for ultra-low bit-widths. In contrast, our work demonstrates that Fused Multiply-Add (FMA)-based approaches, when paired with well-designed microkernels, can achieve near-roofline performance and push the envelope of LLM inference on edge devices.

III. ULTRA LOW-BIT GEMM MICROKERNELS

A. Overview and background

In this section we detail the ultra-low bit GEMM microkernels, that take as input an 1-bit (int1) or 2-bit (int2) weight tensor, multiply it with the input activation tensor and produce the output activations. We refer to this technique as "up-convert and compute". We focus on modern CPUs with AVX2 instructions that can be found on contemporary AI-PC devices, and also on modern Intel GPUs with Xe2 cores that natively support $\text{int2}\times\text{int8}$ operations. As described in Section I, we target the use-cases where the GEMMs illustrate algorithmically very low arithmetic intensity and are typically bandwidth-bound (i.e. single-batch inference). For the CPU case, we implemented all the GEMM microkernels using the `libxsmm` library, a Just-In-Time (JIT) GEMM library that delivers SOTA GEMM performance on CPUs [4], [24]. Our multi-threaded GEMMs for CPUs use these JIT-ed microkernels as building blocks, and for parallelization we leverage `PARLOOPER` and its hybrid scheduling capabilities to fully utilize all performance and efficiency cores [19]. For the Xe2 GPUs, we implement the corresponding low-bit microkernels using the `XeTLA` framework: a collection of SYCL/ESIMD templates that enable high-performance computations on Intel Xe GPU architectures [25].

B. Interleaved Tensor Layout for 2-bit Weights on CPU

Reading 2-bit weights from memory, performing the required multiplications/additions (FMAs), and reaching bandwidth limits is challenging. Naively up-converting the int2 weights to FP32 values (e.g., via look-up tables or permutes) and then multiplying with the input activations requires an excessive number of operations, which diminishes the performance benefits of reading the low-bit data type. CPUs on modern AI PC platforms have a limited number of cores (e.g., 10–20), yet offer bandwidth on the order of 100 GB/s. As a result, the available bandwidth per core is quite high, meaning that simple FP32 FMA throughput is insufficient to saturate the per-core memory bandwidth - especially considering that we read $8\times$ less data than the BF16-equivalent GEMMs while performing the same number of compute operation. This negates the benefits of using the lower-bit datatype.

To address this, we quantize the input activations to int8, allowing us to leverage the int8 VNNI FMAs available on

modern AVX2 CPUs that offer $4\times$ the throughput of FP32 FMAs. The input activation *quantization*, along with the required output activation *dequantization* can be implemented as separate operations before/after the quantized GEMM operations with minimal overhead on the CPUs. More specifically, for memory-bound matrix-vector multiplication scenarios the input and output activations are merely vectors with small size compared to the weight tensors, and as such their quantization and dequantization incur negligible overhead. The int8 VNNI FMA requires the input vector operands to pack together four 8-bit int8 values from the logical contraction dimension of the GEMM (which we denote as K throughout the rest of the paper), and this is the so-called VNNI4 layout. Naively packing together four 2-bit values in the innermost dimension of the weight tensor to effectively form a VNNI4 layout, requires during runtime an excessive number of shifts and shuffles to (i) unpack the int2 values to int8, and (ii) to repack the int8 values back to VNNI4 layout (with a two-level shuffle network) for the upcoming int8-VNNI FMAs.

To alleviate this unpacking bottleneck in the case of 2-bit weights, we introduce a new tensor layout called VNNI4-interleaved, illustrated in Figure 1-Left. In this layout, a logical $M\times K = m32\times k4$ tensor is transformed into an interleaved 3D tensor by folding in the innermost dimension entries from the logical M dimension that are iso-modulo 8. The new tensor layout reflects a 3D tensor $M8\times k4\times m4$ whereas the innermost folded $m4$ dimension corresponds to the originally-indexed $m32$ entries with the same modulo 8 index. In this way, we pack a $[k4][m4]$ 2-bit subtensor in a 32-bit value (see dotted sub-tensor in top of Figure 1-Left), and with a 256-bit vector-load we can read 128 2-bit entries, which effectively form an $[M8][k4][m4]$ tensor.

Using this layout we can simply perform table-lookups that utilize the 2-bit entries as indices and translate them to int8 values that effectively form within a 256-bit vector an $[m8][k4]$ int8 subtensor in VNNI4 format. This int8 vector can be readily used as input to int8 VNNI FMA. In the example of unpack instruction sequence (between the arrows in Figure 1-Left), with the byte-shuffle highlighted in blue `vpshufb ymm3, ymm_lut01, ymm3` we consider the 32 2-bit indices highlighted in blue from the original 2-bit packed vector. The `ymm_lut01` considers only the bits 0-1 of each byte in the vector and maps these indices to the corresponding int8 values. In an analogous way, with the byte-shuffle highlighted in orange `vpshufb ymm4, ymm_lut23, ymm3` we consider the 32 2-bit indices with orange color from the original 2-bit packed vector. The `ymm_lut23` considers only bits 2-3 of each byte in the vector and maps these indices to the proper int8 values. The shift instruction `vpsrld ymm5, ymm3, 0x4` shifts the 4 higher bits 4-7 within each byte to the 4 lower positions such that with 2 more shuffles (highlighted with green and magenta) we can unpack the corresponding int2 values to the respective int8 values. The two logical AND vector operations (`vpand`) in the unpack instruction sequence merely mask out the highest 4 bits within each byte to ensure that the byte-shuffles have the desired

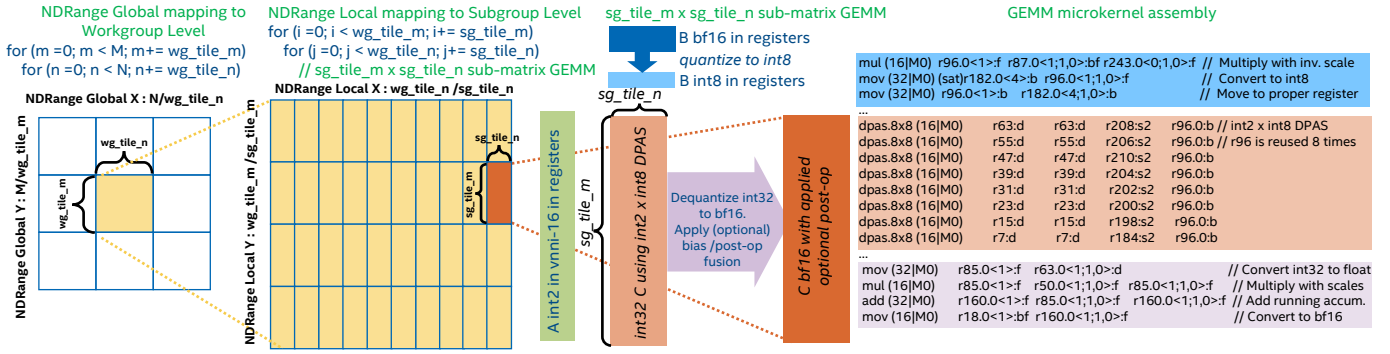


Fig. 3: Xe2 GPU GEMM kernel with int2 weights (A) and BF16 activations (B and C). We split the output matrix $C^{M \times N}$ into tiles with size $wg_tile_m \times wg_tile_n$ and each workgroup will calculate a sub-matrix $wg_tile_m \times wg_tile_n$ (see yellow box at Left). Subsequently, this sub-matrix will be continuously divided into multiple tiles, with dimensions $sg_tile_m \times sg_tile_n$ (see dark-orange rectangular tile). These tiles will then be assigned to subgroups. Finally, the corresponding subgroup GEMM micro-kernel and the involved tile operations will be mapped to the actual Xe2 instructions, such as 2D-load and DPAS instructions (see GEMM microkernel at Right). The quantization of B is fused in the GEMM: while the loaded B sub-matrix is in BF16 (dark-blue box), we quantize the entries to int8 using in-register operations (light-blue assembly box). With rectangular shapes for the $sg_tile_m \times sg_tile_n$ tiles we re-use the quantized B and amortize the corresponding overhead.

`vpbroadcastd ymm3, dword ptr[A]` we broadcast a logical $[m8][k4]$ subtensor of A to within each 32-bit chunk of vector `ymm3`. With an in-lane byte shuffle `vpshufb ymm3, ymm3, ymm_perm` we move the byte containing the i -th bit of the loaded 32-bits to the i -th byte within the 256-bit vector `ymm3`. Then with a logical AND operation `vpand ymm3, ymm1, ymm3` we isolate within each byte the bit residing in the i -th position. After this step, we use a compare instruction `vpcmpeqb ymm3, ymm1, ymm3` to use the previous isolated bits and generate a mask with byte values `0x00` or `0xff` depending on the isolated values of the bits. Last, by using the generated mask we blend with the instruction `vpblendvb ymm3, ymm2, ymm3, ymm3` the int8 values $+1/-1$ to the expanded vector `ymm3`. With such an instruction sequence we upconvert the logical $[m8][k4]$ 1-bit subtensor of A to an $[m8][k4]$ 8-bit subtensor in `ymm3` that has the value $+1$ if the original bit in A is 0 and the value -1 if the original bit in A is 1 (this is the desired weight encoding in our 1-bit weights [2]). With a 32-bit broadcast `vpbroadcastd` we broadcast in `ymm7` four 8-bit values from the input activations B that correspond to 4 elements from the logical K dimension that should be contracted. Finally, with a vnni-int8 FMAs (`vdpbssd ymm12, ymm3, ymm7`) we perform the corresponding multiply-add operations among vectors `ymm3` and vector `ymm7` and we accumulate the partial product in the output 32-bit accumulator `ymm12`. We repeat the same up-convert and FMA sequence for the remaining 96 entries of matrix A (where we reuse the input vector B) and we conclude the int1 GEMM microkernel. With this microkernel as a building block, we compose GEMM and BRGEMM microkernels with larger M , K and N values [26].

E. 2-bit GEMM kernels for Intel Xe2 GPU

Contemporary Xe2 Intel GPUs support natively $\text{int2} \times \text{int8} \rightarrow \text{int32}$ GEMM computations using hardware-

accelerated Dot Product Accumulate Systolic (DPAS) instructions. Therefore, for the Xe2 int2 kernels we can natively use these instructions without the need to upconvert the weights to int8 before performing the necessary multiply-add operations with the int8 activations (cf. with the CPU up-convert& compute methodology). Nevertheless, the SOTA ultra-low bit inference (e.g. 2-bit weights) requires high-precision (e.g. BF16) input/output activations, i.e. the involved GEMM precision is $\text{int2} \times \text{BF16} \rightarrow \text{BF16}$. For the CPU low-precision GEMM, quantizing the input activations from BF16 to int8 before the $\text{int2} \times \text{int8} \rightarrow \text{int32}$ GEMM operation, and dequantizing the int32 GEMM output to BF16 output activations via separate microkernels out of L1/L2 cache adds minimal overhead. More specifically, for memory-bound matrix-vector multiplication scenarios the input and output activations are merely vectors with small size compared to the weight tensors, therefore their quantization and dequantization incur negligible overhead since these operations may run out of L1/L2 cache. However, on GPUs such a decoupled execution (i.e. multiple kernels) of activation-quantization \rightarrow low-precision GEMM microkernel \rightarrow output-dequantization incurs multiple kernel launches and passes over the data.

To mitigate the shortcomings of multiple kernel launches, we developed mixed precision $\text{int2} \times \text{BF16} \rightarrow \text{BF16}$ GEMM Xe2 kernels that fuse the input/output activation quantization/dequantization within the GEMM kernel (see Figure 3). Using conventional SYCL terminology [27], we split the output matrix $C^{M \times N}$ into tiles with size $wg_tile_m \times wg_tile_n$ and each workgroup will calculate a sub-matrix $wg_tile_m \times wg_tile_n$, represented by the yellow box in output C (see Left part of Figure 3). Subsequently, this sub-matrix will be continuously divided into multiple tiles, with dimensions $sg_tile_m \times sg_tile_n$. These tiles will then be

assigned to subgroups. Finally, the corresponding subgroup GEMM microkernel and the involved tile operations will be mapped to the actual Xe2 hardware instructions, such as 2D-load and DPAS instructions. The Xe2 $\text{int2} \times \text{int8} \rightarrow \text{int32}$ DPAS instructions for Xe2 require the int2 operand to be formatted in VNNI16 layout: pack together 16 int2 values from the logical contraction K dimension of the GEMM. Since we are performing inference we can merely pre-format the int2 weights to such VNNI16 layout without any overhead during runtime.

Figure 3 also illustrates the fusion of the input activation (matrix B) quantization and the output quantization. When loading the matrix B from memory in registers, the B precision is BF16 (see dark blue box). In order to quantize the BF16 B entries given some scales B_scales (see blue box in the GEMM microkernel assembly), we first multiply the entries with the inverse of the scales, then we convert the result to int8 (with saturation) and these int8 values (light-blue box) can be readily used in the DPAS instructions (see peach-colored box in microkernel assembly). By carefully selecting the shapes of the $sg_tile_m \times sg_tile_n$ tiles we can reuse the quantized B entries and amortize the corresponding overhead (for the rectangular $sg_tile_m \times sg_tile_n$ tiles of Figure 3 we re-use each quantized B register 8 times). We iterate the same process across all the tiles in the K dimension. Once the full accumulation has been completed (either at the full K granularity or at some user-defined K granularity), we need to dequantize the int32 output registers forming a logical $sg_tile_m \times sg_tile_n$ sub-tensor. First we convert the int32 values to float, then we multiply these float values with the *dequantization* scales and finally we convert the result to BF16 than can be stored to the output C in memory e.g. via 2D-store Xe2 operations (see purple box in microkernel assembly). Also any additional operations (e.g. bias addition, post-GEMM activation functions) can be fused at this point where the C entries are still in-registers before storing them to memory. Our Xe2 GEMM implementation also supports K -splitting algorithms that extract parallelism across the K dimension for smaller GEMM shapes [25].

With respect to the calculation of the B_scales , we have to compute the absolute maximum per quantization granularity (e.g. the absolute max of K B entries or some other user-defined granularity). For this abs-max operation we implemented an optimized SYCL reduction kernel that can be either performed before the GEMM as a separate kernel or it can be fused at the work-group level, and the calculated abs-max values are stored in fast Shared Local Memory (SLM) available on Xe2. Fusing the abs-max B reduction in the GEMM kernel avoids one kernel-launch overhead at the expense of some redundant computations (since multiple work-groups might be performing the same reduction in case they share the same slabs of B). We expose this option of fusing/non-fusing B scale calculation as a tuning knob in our GEMM implementation. Also, the C *dequantization* scales mentioned earlier are merely a product of the corresponding B_scales and the A_scales that are part of the input int2 A

weight matrix.

Last but not least, in order to extract the maximum performance of our int2 Xe2 GEMM kernels for a variety of GEMM shapes and Xe2 platforms, we developed an auto-tuning framework within XeTLA that searches for optimal kernel parameter configurations, e.g. fusing/non-fusing B scale calculation, optimal $wg_tile_m, wg_tile_n, sg_tile_m, sg_tile_n$ tile sizes, using/not-using K -splitting algorithms etc.

F. Performance modeling & limitations of the CPU kernels

The low-precision GEMMs on CPU require additional work to up-convert the low-precision operand to int8 since there is no native hardware support e.g. for $\text{int2} \times \text{int8}$ FMA operations (unlike Xe2 GPUs). Also, the aggregate int8 FMA throughput on modern AI-PC with *limited* number of cores poses a challenge in achieving close to roof-line performance for low-precision CPU GEMMs. In this section we devise roofline models for the 2-bit and 1-bit CPU GEMM microkernels to assess their efficacy and limitations. These models will be used to explain the obtained performance results in section IV. Specifically, we aim to determine under which conditions our CPU microkernels can saturate the available bandwidth on the platform and effectively accelerate matrix-vector multiplications during inference. For our analysis we follow the reasoning/bottleneck-style analysis of the original roofline model [28]. Let β denote the number of bytes/cycle each core in a multi-core CPU can read when all cores access memory simultaneously. Let γ represent the number of cycles to *compute* an output 256-bit vector in the GEMM without considering the data load instructions. Assuming B bytes must be read from memory in order to compute an output 256-bit vector, the number of cycles T to calculate such an output 256-bit vector is:

$$T = \max(B/\beta, \gamma) \quad (1)$$

To operate in a bandwidth-bound regime, since we are reading the weight tensor from memory and the matrix-vector multiplication has no weight re-use, we need the first term in the max operator above to be the dominant one, i.e.:

$$\gamma \leq B/\beta \Rightarrow \beta \leq B/\gamma \quad (2)$$

With this annotation, we can determine the effective bandwidth per core e_{bw} to be bounded by the minimum of the terms β and B/γ (the latter term representing the throughput of the up-convert & compute sequence). In short we can write:

$$e_{bw} = \min(\beta, B/\gamma) \quad (3)$$

Since our CPU platforms have performance P and efficiency E cores with different compute capabilities, we consider two different γ factors, namely γ_P and γ_E , and consequently two different effective bandwidth terms $e_{bw}^P = \min(\beta, B/\gamma_P)$ and $e_{bw}^E = \min(\beta, B/\gamma_E)$. For the 2-bit GEMM microkernel, the γ factor entails the cycles to perform (1 logical shift + 2 logical AND + 4 byte-shuffles + 4 int8

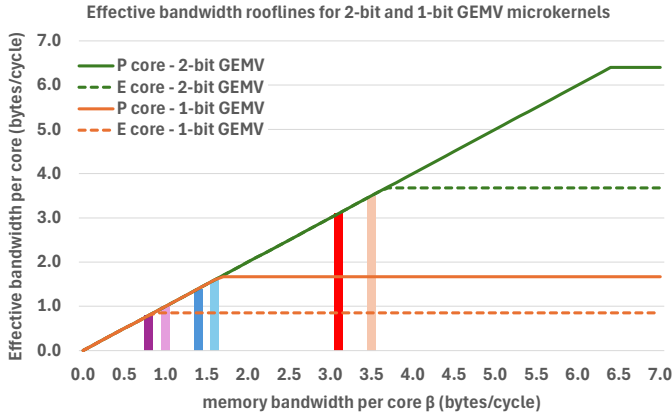


Fig. 4: Effective bandwidth rooflines for 2-bit and 1-bit GEMV microkernels considering P and E cores.

FMA) / 4. In an analogous fashion, for the 1-bit GEMM microkernel, the γ factor entails the cycles to perform (1 byte-shuffle + 1 logical AND + 1 byte-compare + 1 byte-blend + 1 int8 FMA). In either case, we are interested in the throughput of these instruction sequences given the underlying dependencies, and we determined these γ values empirically for both P and E cores on contemporary x86 client CPUs.

Through micro-benchmarks we find that for the 2-bit kernel $\gamma_P = 1.25$ and $\gamma_E = 2.175$. By setting these values in equation 3 and setting $B = 8$ since we need to read 8 bytes to calculate an output 256-bit vector, we obtain: $e_{bw}^P = \min(\beta, 6.4)$ and $e_{bw}^E = \min(\beta, 3.68)$. Figure 4 illustrates the derived rooflines for the effective bandwidth per core in bytes/cycle (y-axis) whereas the x-axis shows the available memory bandwidth per core β in bytes/cycle. The solid green line depicts e_{bw}^P for the 2-bit microkernel whereas the dashed green line corresponds to the e_{bw}^E for the 2-bit microkernel.

Similarly, for the 1-bit kernels we measured $\gamma_P = 2.4$ and $\gamma_E = 4.71$. By setting these values in equation 3 and setting $B = 4$ since we need to read 4 bytes to calculate an output 256-bit vector in the 1-bit case, we obtain: $e_{bw}^P = \min(\beta, 1.7)$ and $e_{bw}^E = \min(\beta, 0.85)$. Figure 4 also illustrates the corresponding e_{bw}^P for the 1-bit microkernel (solid orange line) and e_{bw}^E (dashed orange line). In the next section we use this roofline performance model to analyze the efficacy of our microkernels on our CPU platforms which exhibit β values annotated with vertical bars in Figure 4.

IV. RESULTS

A. Experimental Platforms

For our evaluation we use three contemporary x86 CPUs with varying number of performance and efficiency cores, and different memory bandwidth:

- Intel Core Ultra 9 285K CPU (henceforth referred to as ARL) with 24 cores (8 performance and 16 efficiency cores). It features overclocked memory DDR5@7200 MT/s with measured read bandwidth of 98 GB/s and a Maximum Turbo Power of 250W.
- Intel Core Ultra 7 255H CPU (henceforth referred to as ARLH) with 14 cores (6 performance and 8 efficiency

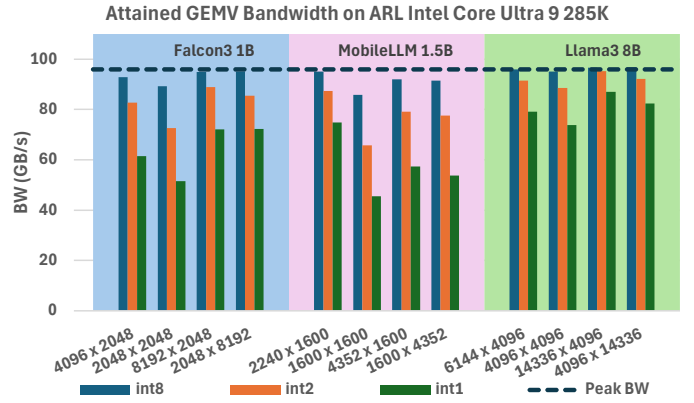


Fig. 5: Attained GEMV bandwidth on ARL for various matrix shapes and precisions (int/int2/int1).

cores). It has memory DDR5@5600 MT/s with measured read bandwidth of 75 GB/s and Maximum Turbo Power of 115W.

- Intel Core Ultra 7 258V CPU (henceforth referred to as LNL) with 8 cores (4 performance and 4 efficiency cores). It has 16GB of DDR5@8533 MT/s memory with measured read bandwidth of 97 GB/s and Maximum Turbo Power of 37W.

For our GPU evaluation we use two Xe2 GPU systems:

- Intel Arc 140V, which is the integrated GPU in the aforementioned Lunar Lake (LNL) platform. It consists of 8 Xe2 GPU cores and it has access to the same memory/bandwidth as the LNL CPU (16 GB of DDR5@8533 MT/s with measured read bandwidth of 97 GB/s).
- Intel Battlemage Arc B580 (BMG) discrete GPU. It consists of 20 Xe2 cores, and it has 12 GB of GDDR6 memory, delivering up to 456 GB/s. The int8 peak is 233 TOPS (Trillions Operations per Second) and its Total Board Power (TBP) is 190W.

B. GEMV microbenchmarks on CPU

In this Section we assess the efficacy of the ultra-low bit GEMV kernels on the aforementioned CPU platforms. For the evaluation, we extracted the weight-matrix shapes from three models: Falcon3-1B [29] model (blue plot areas), MobileLLM-1.5B [30] model (magenta plot areas) and Llama3-8B model [31] (green plot areas). These matrix shapes ($M \times K$) are shown in the x-axis of Figures 5, 6 and 7. The y-axis corresponds to the attained bandwidth (in GB/s) for the corresponding matrix-vector multiplication routines (GEMV), and we show for each matrix shape three bars: i) With dark blue bar we depict the kernels with 8-bit (int8) weights, ii) with orange bars we illustrate the kernels with 2-bit (int2) weights, and iii) with green bars we show the kernels with 1-bit (int1) weights.

In Figure 5 we illustrate the GEMV micro-benchmark results on ARL. As a baseline we consider the int8 GEMM performance where essentially there is no upconvert overhead, and the GEMV microkernel merely consists of vector loads

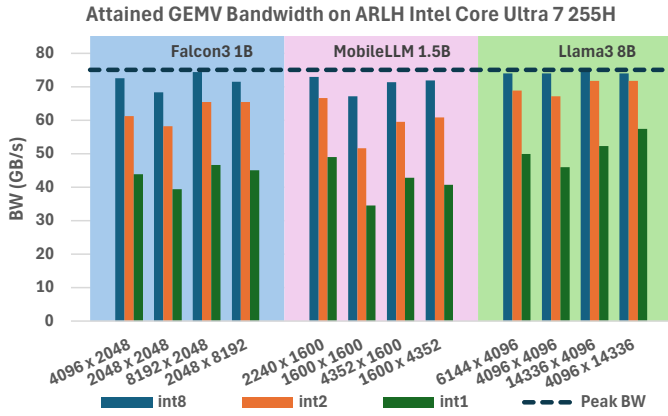


Fig. 6: Attained GEMV bandwidth on ARLH for various matrix shapes and precisions (int/int2/int1).

and vnni-int8 FMAs. The int2 GEMV kernels are within 10–20% of the int8 roofline and achieve bandwidth close to the machine’s peak. Especially for larger matrix sizes (right side of the plot), where the OpenMP and barrier overheads are less significant, the int2 GEMV achieves bandwidth within 2–5% of the int8 GEMV. For the smallest matrix shape 1600×1600 , given the peak read bandwidth (98 Gb/s), the ideal pure int2 microkernel time is 6 microseconds, while we measure 8.9 microseconds. However, OpenMP parallel region fork/join and barrier overheads account for 1 microsecond as measured via benchmarking on ARL. In contrast, the int8 GEMV kernels move $4\times$ more data than the int2 ones, making the relative OpenMP overhead less important. These overheads are even more pronounced for 1-bit weights (dark green bars).

On ARL with total read bandwidth 98 GB/s and 24 cores, each core can draw 4 GB/s assuming equal bandwidth distribution. The operating frequencies of 5.4 Ghz for P cores and 4.5 Ghz for E cores (measured under full load) translate the per-core 4 GB/s to $\beta_P = 0.8$ bytes/cycle per P core and $\beta_E = 0.95$ bytes/cycle per E core (see dark magenta and light magenta vertical bars in Figure 4). According to the roofline performance model, both P and E cores with the 2-bit kernel should achieve peak bandwidth (since we are residing in the slanted parts of the roofline, see green lines), which aligns with our GEMV benchmark results. Similarly, for 1-bit kernels (orange lines), P cores operate in the slanted region, while E cores are near the knee of the dotted orange line. This suggests that 1-bit GEMV on ARL should deliver near-peak bandwidth, modulo OpenMP overheads.

Figure 6 shows GEMV results on ARLH. The conclusions are similar to ARL: int2 GEMV kernels are within 10–20% of the int8 roofline and achieve near-peak bandwidth. With 75 GB/s total bandwidth and 14 cores, each core can draw 5.36 GB/s assuming equal bandwidth distribution. The operating frequencies of 4 GHz (P cores) and 3.6 GHz (E cores) yield $\beta_P = 1.44$ and $\beta_E = 1.6$ bytes/cycle (see dark and light blue vertical bars in Figure 4). For the 2-bit GEMV case, both P and E cores are modeled to hit peak bandwidth (slanted green lines), and it is confirmed by our GEMV benchmarks. For the 1-bit GEMV case, P cores saturate the available bandwidth

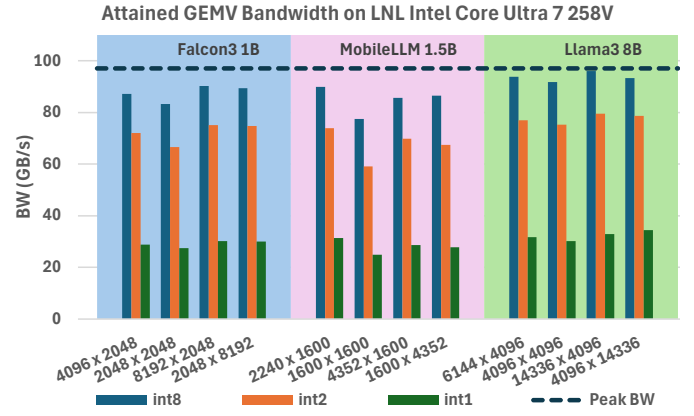


Fig. 7: Attained GEMV bandwidth on LNL for various matrix shapes and precisions (int/int2/int1).

(dark blue bar intersects slanted orange line in Figure 4), while E cores are limited by the upconvert-and-compute sequence (light blue bar intersects first flat part of dotted orange line). This means E cores on ARLH with 1-bit kernels can read up to 0.85 bytes/cycle or 2.85 GB/s. With 6 P and 8 E cores, the modeled bandwidth is 55 GB/s, closely matching observed values for larger matrices (dark green bars in Figure 6).

Finally, Figure 7 shows the GEMV microbenchmarks on the LNL platform. We observe that the 2-bit microkernel continues to deliver performance close to the theoretical peak (within 20–25% for the larger matrix shapes), while the 1-bit GEMV yields consistently lower performance, around 30 GB/s across all cases. On LNL, with a total read bandwidth of 97 GB/s and 8 cores, the per-core bandwidth is approximately 12.1 GB/s. The measured operating frequencies of 4.1 GHz for P cores and 3.7 GHz for E cores translate to $\beta_P = 3.18$ bytes/cycle and $\beta_E = 3.52$ bytes/cycle (see dark red and light red vertical bars in Figure 4). For the 2-bit GEMV kernels, we conclude that both P and E cores are able to reach close to peak read bandwidth, which is confirmed by the GEMV microbenchmark results. However, for the 1-bit GEMV kernels, both P and E cores are limited by the upconvert-and-compute sequence, as indicated by the vertical red bars intersecting first the flat regions of the solid and dotted orange rooflines. As a result, the effective bandwidth for the 1-bit kernel on LNL is limited to 6.5 GB/s per P core and 2.92 GB/s per E core, yielding a total modeled bandwidth of approximately 37 GB/s (4 P + 4 E cores). This explains the relatively poor performance of the 1-bit GEMV microbenchmarks on LNL. In conclusion, on LNL that offers relatively high read bandwidth and only 8 cores, the 1-bit kernels are unable to saturate the available bandwidth. The upconvert-and-compute sequence becomes the bottleneck, limiting the overall performance of 1-bit GEMV kernels.

C. GEMV/GEMM microbenchmarks on Intel Xe2 GPUs

In this section we present analogous GEMV microbenchmarks for our Xe2 GPU systems. In addition to the memory bound GEMV microbenchmarks ($N = 1$), we present here microbenchmarks results for GEMM shapes with larger N

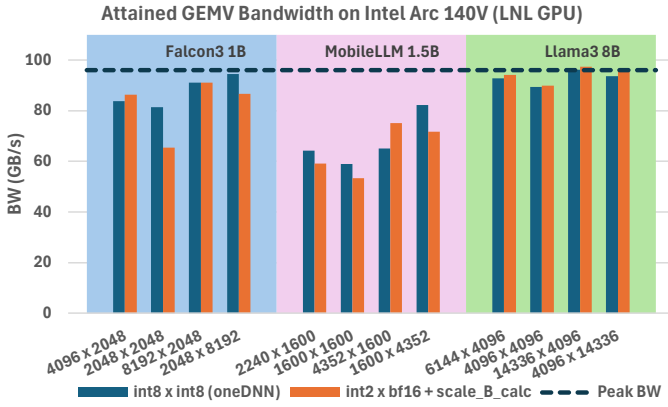


Fig. 8: Attained GEMV bandwidth on LNL-GPU for various matrix shapes and precisions (weights int2/int8).

dimension that should lead to compute bound kernels. The contemporary Xe2 systems offer high compute throughput via the $\text{int}2 \times \text{int}8 \rightarrow \text{int}32$ DPAS instructions (same as the $\text{int}8 \times \text{int}8 \rightarrow \text{int}32$ throughput, e.g. ≈ 50 TFLOPS for the integrated Intel Arc 140V and ≈ 200 TFLOPS for Battlemage B580), and as such should be able to accelerate the compute bound/prefill phases of the $\text{int}2$ inference compared to the pure BF16 inference. Therefore, we will also assess the efficacy of our mixed precision $\text{int}2 \times \text{BF}16 \rightarrow \text{BF}16$ Xe2 GPU kernels for compute-bound GEMM cases.

In Figure 8 we illustrate the GEMV micro-benchmark results on the integrated Intel Arc 140V (LNL-GPU). As a baseline (blue bars) we consider the $\text{int}8 \times \text{int}8$ GEMV performance from oneDNN where essentially there is no input/output quantization/dequantization overheads. The $\text{int}2 \times \text{BF}16 \rightarrow \text{BF}16$ GEMV kernels (including the calculation of the B scales) are within 10% of the $\text{int}8$ roofline and achieve bandwidth close to the machine’s peak (see orange bars). Especially for larger matrix sizes (right side of the plot), where the kernel launch overheads are less significant, the $\text{int}2$ GEMV achieves bandwidth same as the $\text{int}8$ GEMV. For the smallest matrix shape 1600×1600 , given the peak read bandwidth (98 Gb/s), the ideal pure $\text{int}2$ microkernel time is 6 microseconds. However, the kernel launch overhead is in the order of 2 microseconds, thus we effectively observe 53 Gb/s bandwidth. We also observe that the sustained bandwidth by the $\text{int}2$ Xe2 LNL-GPU kernels is comparable and slightly higher than the one achieved by the LNL-CPU cores (see Figure 7). This is expected since both CPU and Xe2 CPU have access to the same DDR5 memory and the Xe2 kernels with the native $\text{int}2 \times \text{int}8$ DPAS instructions are able to alleviate some of the upconvert overheads that exist on the CPU kernels. We note that for all the GEMV cases, we found experimentally that fusing the B scale calculation within the kernel (in order to avoid separate kernel launches at the expense of redundant computation) is beneficial, especially since the B tensor is merely an activation vector. All these results indicate that our fused $\text{BF}16 \rightarrow \text{BF}16$ Xe2 kernels described in Section III-E are able to effectively hide the quantization/dequantization overheads and achieve close to peak memory bandwidth.

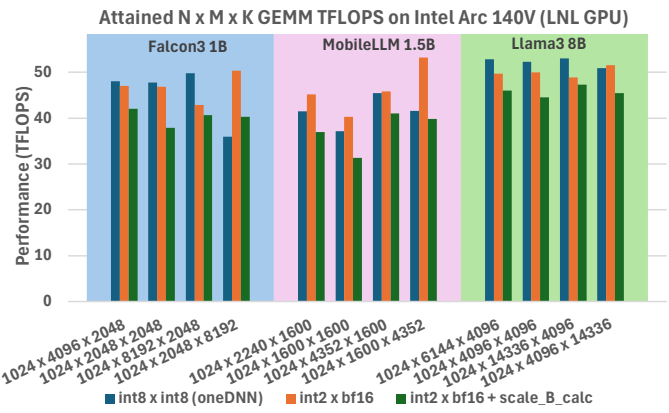


Fig. 9: Attained GEMM TFLOPS on LNL-GPU for various matrix shapes and precisions (weights int2/int8).

Figure 9 shows the attained GEMM performance ($N = 1024$) for the same weight matrices as the ones in the previous microbenchmarks. These GEMM have substantially higher weight re-use compared to the GEMV cases and in principle should be compute bound. To shed light on the obtained performance we illustrate the obtained performance in TFLOPS for 3 different configurations: i) a pure $\text{int}8 \times \text{int}8$ GEMM from oneDNN without any quantization/dequantization overheads that should serve as attainable roofline (blue bars), ii) the fused $\text{int}2 \times \text{BF}16 \rightarrow \text{BF}16$ Xe2 GEMM kernel only (illustrated in Figure 3, i.e. without the kernel/pass for calculating the B scales) depicted with orange bars, and iii) the full-fledged mixed precision $\text{int}2$ GEMM including the overhead of calculating the B scales via a separate kernel (green bars). First of all, we observe that the fused mixed precision $\text{int}2$ GPU GEMM kernels described in Section III-E achieve performance close to the pure $\text{int}8 \times \text{int}8$ GEMM (note that the $\text{int}2 \times \text{int}8$ DPAS instruction has the same throughput as the $\text{int}8 \times \text{int}8$ DPAS instruction). This result highlights the efficacy of our fused implementation that essentially hides all the online quantization and dequantization computations. For these *compute-bound* GEMMs where the input activations are not simply a vector, we found experimentally that the best performance is obtained by performing the input B scale calculation as a *separate kernel* before the GEMM (instead of fusing this B scale calculation in the GEMM kernel like we did in the GEMV cases). This overhead is typically in the range of 5-15% and for the cases with larger M it is diminished down to 3%. Finally comparing the *full* mixed precision kernel performance (green bars) with the performance of the pure $\text{int}8$ kernels from oneDNN serving as an attainable roofline (blue bars), we observe that the $\text{int}2 \times \text{BF}16 \rightarrow \text{BF}16$ Xe2 GEMMs are within 5-15% of the pure $\text{int}8$ oneDNN GEMMs. For the larger tested matrices/shapes, we achieve on LNL-GPU up to 47 TFLOPS with the full-fledged $\text{int}2$ GEMM (whereas the maximum achieved is 53 TFLOPS by the $\text{int}8$ GEMM, essentially being close to $\approx 90\%$ of the attainable peak). For comparison, LNL-CPU cores have a peak aggregate $\text{int}8$ FMA throughput of ≈ 1.7 TFLOPS, therefore using the $\text{int}2$ GEMM kernels on LNL-GPU Xe2 cores enable

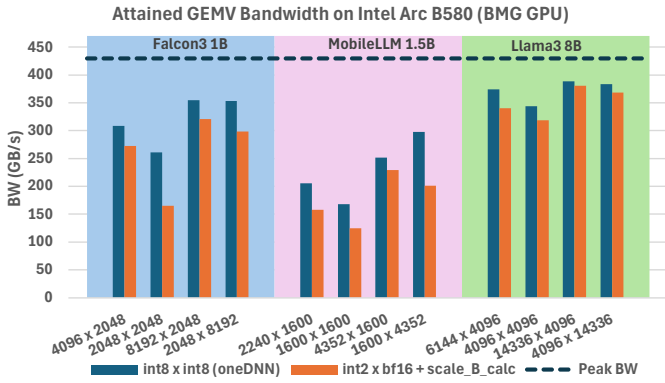


Fig. 10: Attained GEMV bandwidth on BMG-GPU for various matrix shapes and precisions (weights int2/int8).

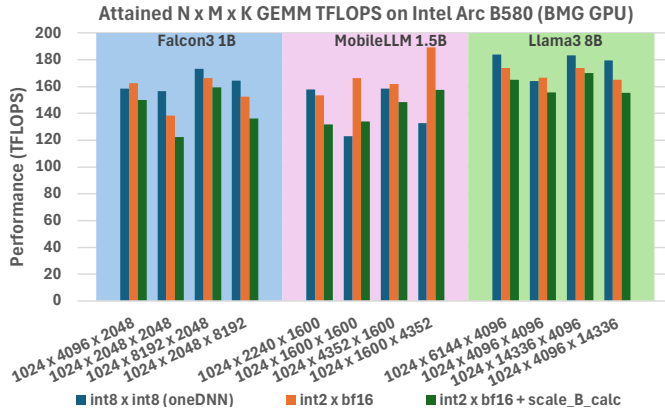


Fig. 11: Attained GEMM TFLOPS on BMG-GPU for various matrix shapes and precisions (weights int2/int8).

substantial benefits for compute bound use-cases (e.g. prefill inference stage, larger batch size).

Figures 10 and 11 illustrate the analogous GEMV and GEMM results on the BMG discrete GPU, and the conclusions are similar to the ones for the LNL-GPU case: For both GEMV and GEMM cases the mixed precision int2 \times BF16 \rightarrow BF16 Xe2 GEMM achieves performance close to the pure int8 \times int8 GEMM from oneDNN which serves as an attainable roofline. Especially for larger matrices (right side of the plots), the obtained performance for the ultra-low bit kernels is within 5-10% of the roofline, effectively showing that our fused kernel implementation diminishes the necessitated quantization and dequantization overheads. For the larger GEMV cases occurring in Llama3-8B model, BMG achieves bandwidth up to 380 GB/s and for the corresponding GEMM cases ($N = 1024$) we achieve up to 175 TFLOPS via our mixed precision implementation. We note here that due to the increased bandwidth of BMG (~ 450 Gb/s vs ~ 97 GB/s on LNL-GPU) the kernel launch overheads are more emphasized for the cases where the involved matrices are small (e.g. MobileLLM-1.5B model).

D. End to end inference results on CPU

We integrated our multi-threaded 2-bit and 1-bit GEMMs into the optimized PyTorch-TPP framework, which delivers

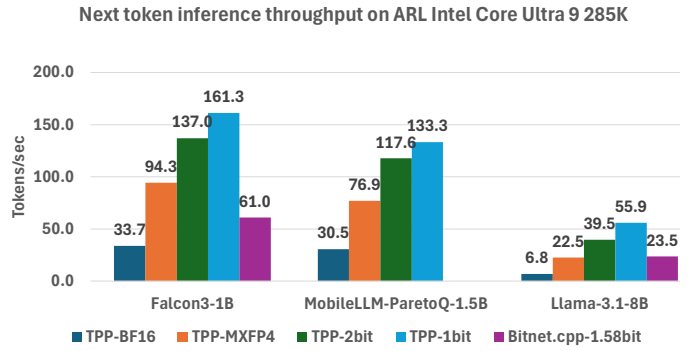


Fig. 12: End-to-end inference on ARL. For the inference with PyTorch-TPP we have four variants: (i) Dark blue bars correspond to BF16 weights. (ii) Orange bars correspond to MXFP4 weights, (iii) Green bars correspond to 2-bit weights, (iv) Light blue bars correspond to 1-bit weights. With magenta bars we represent the performance of the bitnet.cpp framework.

state-of-the-art inference performance on CPUs [19]. For evaluation, we focus on three LLM models: Falcon3-1B [29], MobileLLM-1.5B [30], and Llama3-8B [31]. The MobileLLM family, released by Meta as a companion to the recent ParetoQ work, is truly quantized to 2-bit and 1-bit using QAT techniques, achieving state-of-the-art accuracy for their respective model sizes [2]. The same QAT techniques have been applied to Llama3 models, producing high-accuracy 1-bit and 2-bit variants, although the weights have not yet been released. Therefore, for performance evaluation, we use dummy 1-bit/2-bit weights for Llama3-8B. Since bitnet.cpp has limited model coverage, we include Falcon3-1B (which is supported by bitnet.cpp) as the smallest benchmarked model and also use dummy 1-bit/2-bit weights for performance runs. All experiments generate 128 output tokens with batch size 1. For bitnet.cpp, we test various core configurations and report the best result. Additionally, since PyTorch-TPP supports MXFP4 (4-bit) Weight-Only Quantization (WOQ), we benchmark this variant as well [32].

Figure 12 illustrates the end-to-end inference results on ARL. For the inference with PyTorch-TPP we have four variants: (i) Dark blue bars correspond to BF16 weights. (ii) Orange bars correspond to MXFP4 weights, (iii) Green bars correspond to 2-bit weights, (iv) Light blue bars correspond to 1-bit weights. With magenta bars we represent the performance of the bitnet.cpp framework. The measured performance is in tokens/second (y-axis). First of all, we observe that the 4-bit inference with PyTorch-TPP is faster than bitnet.cpp on the 1B parameter model and on par with bitnet.cpp for the 8B model, even though bitnet.cpp uses 2-bit weights (and as such should be substantially faster than the 4-bit inference). These results suggest that bitnet.cpp is far from optimal. In our case, we observe with our optimized 2-bit inference substantial speedups over the 16-bit baseline, more precisely $4.1\times$, $3.9\times$ and $5.8\times$ for the respective 1B, 1.5B and 8B models. With 1-bit inference we further accelerate the end-to-end pipeline over the 16-bit case by factors $4.8\times$, $4.4\times$ and $8.3\times$ for the respective 1B, 1.5B and 8B models.

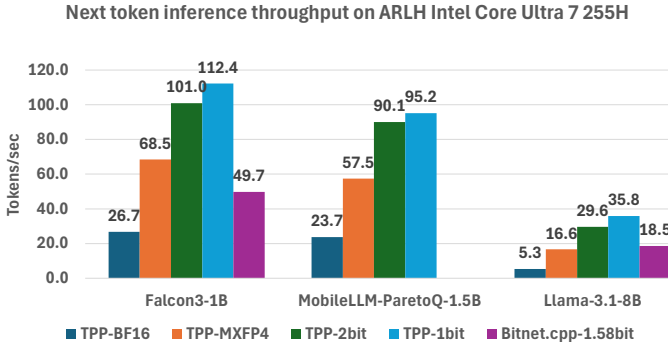


Fig. 13: End-to-end inference on ARLH.

To understand these results, let us derive some performance models. More specifically, given the end-to-end inference execution we know that only the GEMV portions can be accelerated with our new kernels. Assuming that in the 16-bit inference execution the GEMV kernels constitute a fraction α of the total execution time, and by applying the reasoning of Amdahl’s law, the maximum attainable speedup s over the 16-bit inference by using a datatype x times smaller is:

$$s = \frac{1}{1 - \alpha + \frac{\alpha}{x}} \quad (4)$$

For the 1B model, in the 16-bit run on ARL we get $\alpha = 0.87$ (i.e. 87% of the time is spent in the GEMVs), and as a result the maximum attainable speedup is $4.3\times$ for the 2-bit inference ($x = 8$) and $5.5\times$ for the 1-bit inference ($x = 16$). Under this lens, we indeed see that our obtained results are close to the ideal ones (we observed $4.1\times$ and $4.8\times$ respectively). On the other extreme with the 8B model, in the 16-bit run we get on ARL $\alpha = 0.96$ (i.e. 96% of the time is spent in the GEMVs), and consequently the maximum attainable speedup is $6.1\times$ for the 2-bit inference ($x = 8$) and $9.6\times$ for the 1-bit inference ($x = 16$). Again we see that our obtained results are close to the ideal ones (we observed $5.8\times$ and $8.3\times$ speedup over the 16-bit baseline).

When comparing our 2-bit inference with the 1.58-bit inference of bitnet.cpp we observe on ARL speedups of $2.2\times$ for the 1B model and $1.7\times$ for the 8B case, showing that our optimized 2-bit kernels along with the PyTorch-TPP runtime are improving substantially the SOTA 2-bit inference on CPUs.

Figure 13 exhibits the end-to-end inference results on ARLH. The high level picture is similar to the one described in the ARL case: we observe with our optimized 2-bit inference speedups over the 16-bit baseline, more precisely $3.8\times$, $3.8\times$ and $5.6\times$ for the respective 1B, 1.5B and 8B models. With 1-bit inference we further accelerate the end-to-end pipeline over the 16-bit case by factors $4.2\times$, $4\times$ and $6.8\times$ for the respective 1B, 1.5B and 8B models. When comparing our 2-bit inference with the 1.58-bit inference of bitnet.cpp we observe on ARLH speedups of $2\times$ for the 1B model and $1.6\times$ for the 8B case.

Figure 14 depicts the end-to-end inference results on LNL. We observe with our optimized 2-bit inference speedups over the 16-bit baseline, more precisely $3.8\times$, $3.5\times$ and $7\times$ for the respective 1B, 1.5B and 8B models. For the 1-bit case however,

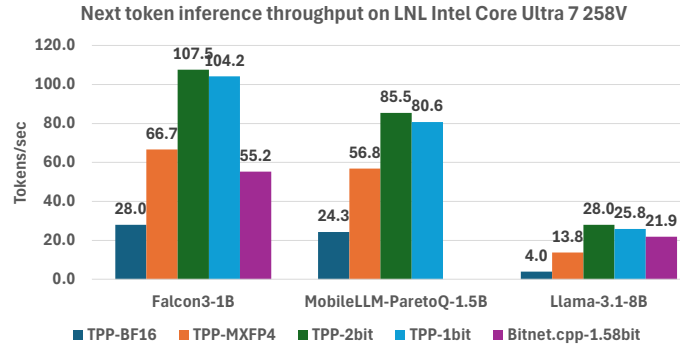


Fig. 14: End-to-end inference on LNL.

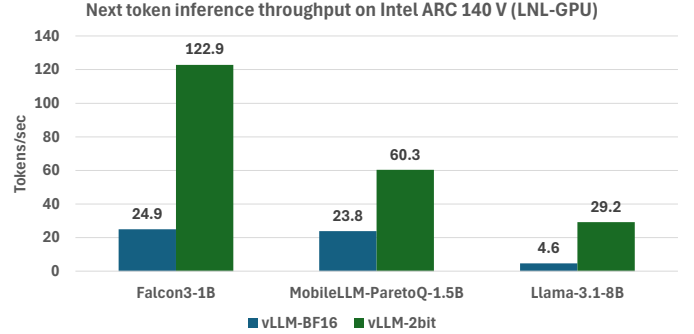


Fig. 15: End-to-end inference on LNL-GPU.

we are not observing any further speedups; this behavior is completely justified by the 1-bit GEMV microbenchmark results analyzed in section IV-B. On LNL with relatively high read bandwidth available and only 8 cores, the 1-bit kernels can not saturate the full available bandwidth and the upconvert & compute sequence is the bottleneck. When comparing our 2-bit inference with the 1.58-bit inference of bitnet.cpp we observe on LNL speedups of $1.9\times$ for the 1B model and $1.3\times$ for the 8B case.

E. End to end inference results on Intel Xe2 GPUs

For the evaluation of the end to end inference with the Intel Xe2 GPUs, we integrated our optimized kernels into the vLLM [5] framework as a quantization plugin and evaluated the inference on the same datasets and setup described in Section IV-D. Figure 15 exhibits the end to end inference on LNL-GPU with BF16 precision (blue bars) and 2-bit weights (green bars), and we observe that the 2-bit inference provides speedup up to $6.3\times$ for the inference with the Llama3-8B model, achieving for this case 29.2 tokens/second. As expected, this throughput is in alignment with the obtained LNL-CPU result (~ 28 tokens/sec) since both CPU and Xe2 GPU on the LNL platform have access to the same bandwidth. However, on the LNL AI-PC platform one can benefit from leveraging the Xe2 GPU in compute-bound use-cases like inference with longer context, larger batch size and shorter output length, since the compute-bound GEMM performance gap of LNL-CPU and LNL-GPU is $\sim 30\times$ as illustrated in Section IV-C. We ran an experiment with the 2-bit Llama3-8B model, 2048 input tokens and 16 output tokens, and we

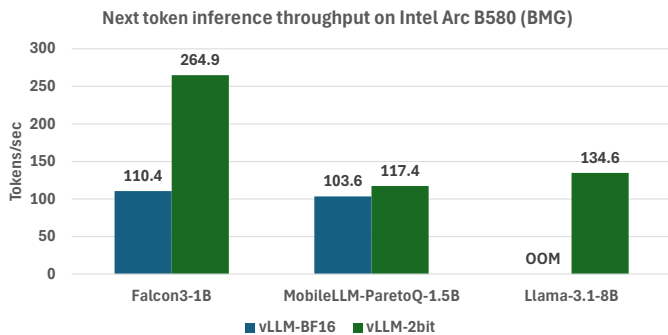


Fig. 16: End-to-end inference on BMG-GPU.

observed that LNL-GPU is $\sim 26\times$ faster than LNL-CPU with respect to the end to end latency.

Figure 16 illustrates the end to end inference on BMG for the same experimental setup. The largest BF16 model (Llama3-8B) does not fit in the memory of BMG (12 GB) and as such we denote that point with “OOM” (Out-Of-Memory) in the plot. On the other hand, our 2-bit Llama3-8B model requires only ~ 2 GB of memory, and on BMG the int2 end to end inference with our Xe2 kernels obtains ~ 135 tokens/sec. As a sanity check, this performance on BMG is $\sim 4.6\times$ higher than the one obtained on LNL-GPU, which is in alignment with their relative $4.7\times$ gap in the bandwidth. For the case with the smaller MobileLLM-1.5B model, the observed speedup on BMG is only $1.1\times$. We shed light on this behavior by looking at the detailed breakdown of the inference. For this model, our detailed breakdown shows that the GEMV kernels on the GPU device are indeed accelerated by $\sim 3\times$ (compared to BF16) which is in alignment with the GEMV microbenchmarks of Figure 10 (middle bars). However, end-to-end inference latency has one more component, where CPU scheduling and synchronization time plays a critical role. Our optimized int2 Xe2 kernels reduce the GPU device time substantially, and as a result the CPU scheduling time gets exposed, impacting the overall speedup. More specifically, the CPU overheads for such cases with very small involved matrices are increased by $3.6\times$ compared to the BF16 inference. These CPU overheads are exposed and can not be hidden fully behind the int2 GEMV kernels with very small device time, negating the benefits obtained in pure device time in GEMV.

F. CPU comparison with 2-bit inference on NVIDIA GPU

In a recent update, bitnet.cpp included CUDA optimized 2-bit kernels tailored for the NVIDIA A100 platform, and we were able to reproduce the reported results in that repo¹ on our local A100 GPU. To have an apples-to-apples comparison with our CPU results, we benchmarked our 2-bit inference pipeline on a same-size 2 Billion parameter model². On the A100 GPU and with the bitnet-b1.58 2 Billion model we were able to obtain 250 tokens/s, whereas we achieve on the aforementioned same-sized 2B model 110 tokens/s on ARL, 82 tokens/s on ARLH, and 88 tokens/s on LNL. As

¹<https://github.com/microsoft/BitNet/tree/main/gpu>

²<https://huggingface.co/andrijdavid/Llama3-2B-Base>

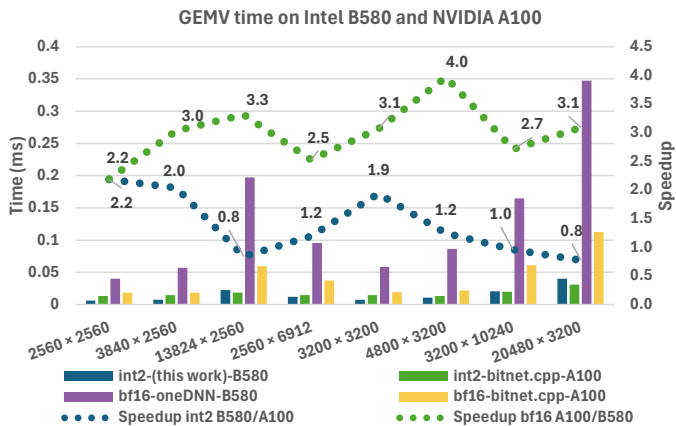


Fig. 17: GEMV execution time on A100 and B580 (BMG) for various matrix configurations (x-axis) and precisions.

a result, we conclude that this level of performance on the CPUs is within $2.3\times$ - $3\times$ of the A100 GPU which has $17\times$ - $20\times$ more bandwidth than our CPUs. To further shed light on these results, we assessed the efficacy of the 2-bit GEMV kernels on A100 compared to the corresponding 16-bit ones (these results are also provided in the bitnet.cpp and we were able to reproduce them). On the A100 GPU, for the smaller matrix shapes (e.g. 2560×2560 , 3840×2560 , 3200×3200) the observed 2-bit GEMV speedup over the 16-bit GEMV is only $1.3\times$ - $1.4\times$ whereas for the larger shapes the speedup goes up to $3.6\times$ (see Figure 17, bf16 GEMV performance on A100 with yellow bars and int2 GEMV on A100 with green bars). Considering that the majority of matrices in such LLMs (i.e. 2B) are relatively small, we expect the upside of the 2-bit GEMVs to be limited on A100. For comparison, in similarly-sized matrices we were able to observe close to ideal bandwidth with our 2-bit GEMV kernels on CPUs, meaning that they are $\approx 7\times$ faster than the corresponding 16-bit GEMVs, and as a result we materialized substantial speedup in the end-to-end 2-bit inference.

G. BMG comparison with 2-bit inference on NVIDIA GPU

Finally, we compare the 2-bit end to end inference performance on B580 (BMG) with the A100 2-bit inference from bitnet.cpp on a same-sized 2 B model (same setup as the one in Section IV-F). On BMG we obtained 365 tokens/sec, essentially being $1.46\times$ faster than the 2-bit inference on A100 despite the fact that BMG has almost $4\times$ less bandwidth than A100. To understand this behavior, we illustrate in Figure 17 the GEMV execution times for various shapes and precisions on both BMG and A100. First by comparing the BF16 GEMV times (magenta bars for BMG and yellow bars for A100) we observe that A100 is for larger matrices 3 - $4\times$ faster than BMG, which aligns with the $4\times$ gap in the bandwidth among the two platforms (see green dotted speedup line). However, when comparing the int2/2-bit GEMV times (blue bars for BMG and green bars for A100) the landscape changes: BMG is up to $2.2\times$ faster than A100 (see blue dotted speedup line) despite having less available bandwidth. The efficiency of our

2-bit Xe2 GEMV kernels (e.g. see Figure 10) is substantially better than the ones of the 2-bit A100 GEMV kernels (which show only limited speedup of $1.3\times$ - $1.4\times$ over the BF16 GEMV for smaller matrix shapes). As a result, the 2-bit end-to-end inference on BMG ends up being faster than the 2-bit inference on A100 for a 2B parameter model.

V. CONCLUSIONS AND FUTURE WORK

In this work, we designed and implemented 1-bit and 2-bit GEMM microkernels optimized for modern x86 CPUs, achieving close to roof-line efficiency across a variety of CPU platforms. We integrated these microkernels into a state-of-the-art LLM inference framework and presented end-to-end inference results with 2-bit models that outperform the current SOTA runtime (bitnet.cpp) by up to $2.2\times$, and deliver up to $7\times$ speedup compared to the 16-bit model inference. We then extend this work to Intel GPUs where we design and implement mixed precision, 2-bit GEMM kernels, and show their performance to be close to optimal, speeding up the BF16 inference up to $6.3\times$. On a discrete Intel Arc B580 Xe2 GPU we achieve a speedup of $1.5\times$ over the 2-bit inference on A100 for a same-sized 2 Billion parameter model, despite A100 having $4\times$ more bandwidth than B580. Thus, our work pushes the envelope of LLM inference on AI-PCs and Intel Xe GPUs, and demonstrates that ultra-low-bit inference even on CPUs and discrete client GPUs can approach high-end GPU-level performance. As future work we plan to extend our work to ARM platforms, since essentially our 1-bit and 2-bit microkernels can be readily translated to AArch64 and SVE instructions which are available on modern ARM CPUs.

REFERENCES

- [1] Shuming Ma, Hongyu Wang, Lingxiao Ma, Lei Wang, Wenhui Wang, Shaohan Huang, Li Dong, Ruiping Wang, Jilong Xue, and Furu Wei. The era of 1-bit llms: All large language models are in 1.58 bits, 2024.
- [2] Zechun Liu, Changsheng Zhao, Hanxian Huang, Sijia Chen, Jing Zhang, Jiawei Zhao, Scott Roy, Lisa Jin, Yongyang Xiong, Yangyang Shi, et al. Paretoq: Scaling laws in extremely low-bit llm quantization. *arXiv preprint arXiv:2502.02631*, 2025.
- [3] Jinheng Wang, Hansong Zhou, Ting Song, Shijie Cao, Yan Xia, Ting Cao, Jianyu Wei, Shuming Ma, Hongyu Wang, and Furu Wei. Bitnet.cpp: Efficient edge inference for ternary llms, 2025.
- [4] Evangelos Georganas, Dhiraj Kalamkar, Sasikanth Avancha, Menachem Adelman, Cristina Anderson, Alexander Breuer, Jeremy Bruestle, Narendra Chaudhary, Abhisek Kundu, Denise Kutnick, et al. Tensor processing primitives: A programming abstraction for efficiency and portability in deep learning workloads. In *Proceedings of the International Conference for High Performance Computing, Networking, Storage and Analysis*, pages 1–14, 2021.
- [5] Woosuk Kwon, Zhuohan Li, Siyuan Zhuang, Ying Sheng, Lianmin Zheng, Cody Hao Yu, Joseph Gonzalez, Hao Zhang, and Ion Stoica. Efficient memory management for large language model serving with pagedattention. In *Proceedings of the 29th symposium on operating systems principles*, pages 611–626, 2023.
- [6] Marcos Treviso, Ji-Ung Lee, Tianchu Ji, Betty van Aken, Qingqing Cao, Manuel R Ciosici, Michael Hassid, Kenneth Heafield, Sara Hooker, Colin Raffel, et al. Efficient methods for natural language processing: A survey. *Transactions of the Association for Computational Linguistics*, 11:826–860, 2023.
- [7] Elias Frantar and Dan Alistarh. Sparsegpt: Massive language models can be accurately pruned in one-shot. In *International Conference on Machine Learning*, pages 10323–10337. PMLR, 2023.
- [8] Geoffrey Hinton, Oriol Vinyals, and Jeff Dean. Distilling the knowledge in a neural network. *arXiv preprint arXiv:1503.02531*, 2015.
- [9] Rohan Taori, Ishaan Gulrajani, Tianyi Zhang, Yann Dubois, Xuechen Li, Carlos Guestrin, Percy Liang, and Tatsunori B Hashimoto. Stanford alpaca: An instruction-following llama model, 2023.
- [10] Ji Lin, Jiaming Tang, Haotian Tang, Shang Yang, Wei-Ming Chen, Wei-Chen Wang, Guangxuan Xiao, Xingyu Dang, Chuang Gan, and Song Han. Awq: Activation-aware weight quantization for on-device llm compression and acceleration. *Proceedings of Machine Learning and Systems*, 6:87–100, 2024.
- [11] Jerry Chee, Yaohui Cai, Volodymyr Kuleshov, and Christopher M De Sa. Quip: 2-bit quantization of large language models with guarantees. *Advances in Neural Information Processing Systems*, 36:4396–4429, 2023.
- [12] Zechun Liu, Changsheng Zhao, Hanxian Huang, Sijia Chen, Jing Zhang, Jiawei Zhao, Scott Roy, Lisa Jin, Yongyang Xiong, Yangyang Shi, et al. Paretoq: Scaling laws in extremely low-bit llm quantization. *arXiv preprint arXiv:2502.02631*, 2025.
- [13] Jiedong Lang, Zehao Guo, and Shuyu Huang. A comprehensive study on quantization techniques for large language models. In *2024 4th International Conference on Artificial Intelligence, Robotics, and Communication (ICAIRC)*, pages 224–231. IEEE, 2024.
- [14] Jordan Hoffmann, Sebastian Borgeaud, Arthur Mensch, Elena Buchatskaya, Trevor Cai, Eliza Rutherford, Diego de Las Casas, Lisa Anne Hendricks, Johannes Welbl, Aidan Clark, et al. Training compute-optimal large language models. *arXiv preprint arXiv:2203.15556*, 2022.
- [15] Tanishq Kumar, Zachary Ankner, Benjamin F Spector, Blake Bordelon, Niklas Muennighoff, Mansheej Paul, Cengiz Pehlevan, Christopher Ré, and Aditi Raghunathan. Scaling laws for precision. *arXiv preprint arXiv:2411.04330*, 2024.
- [16] Tim Dettmers and Luke Zettlemoyer. The case for 4-bit precision: k-bit inference scaling laws. In *International Conference on Machine Learning*, pages 7750–7774. PMLR, 2023.
- [17] Zechun Liu, Barlas Oguz, Aasish Pappu, Yangyang Shi, and Raghuraman Krishnamoorthi. Binary and ternary natural language generation. *arXiv preprint arXiv:2306.01841*, 2023.
- [18] Georgi Gerganov. llama.cpp: Llm inference in c/c++, <https://github.com/ggml-org/llama.cpp>.
- [19] Evangelos Georganas, Dhiraj Kalamkar, Kirill Voronin, Abhisek Kundu, Antonio Noack, Hans Pabst, Alexander Breuer, and Alexander Heinecke. Harnessing deep learning and hpc kernels via high-level loop and tensor abstractions on cpu architectures. In *2024 IEEE International Parallel and Distributed Processing Symposium (IPDPS)*, pages 950–963. IEEE, 2024.
- [20] Darshan C Ganji, Saad Ashfaq, Ehsan Saboori, Sudhakar Sah, Saptarshi Mitra, Mohammadhossein Askarihemmat, Alexander Hoffman, Ahmed Hassanien, and Mathieu Leonardon. Deepgemm: Accelerated ultra low-precision inference on cpu architectures using lookup tables. In *Proceedings of the IEEE/CVF conference on computer vision and pattern recognition*, pages 4656–4664, 2023.
- [21] Davis Blalock and John Guttag. Multiplying matrices without multiplying. In *International Conference on Machine Learning*, pages 992–1004. PMLR, 2021.
- [22] Xiaohu Tang, Yang Wang, Ting Cao, Li Lina Zhang, Qi Chen, Deng Cai, Yunxin Liu, and Mao Yang. Lut-nn: Empower efficient neural network inference with centroid learning and table lookup. In *Proceedings of the 29th Annual International Conference on Mobile Computing and Networking*, pages 1–15, 2023.
- [23] Jianyu Wei, Shijie Cao, Ting Cao, Lingxiao Ma, Lei Wang, Yanyong Zhang, and Mao Yang. T-mac: Cpu renaissance via table lookup for low-bit llm deployment on edge, 2024. URL <https://arxiv.org/abs/2407.00088>.
- [24] Alexander Heinecke, Greg Henry, Maxwell Hutchinson, and Hans Pabst. Libxsmm: accelerating small matrix multiplications by runtime code generation. In *SC'16: Proceedings of the International Conference for High Performance Computing, Networking, Storage and Analysis*, pages 981–991. IEEE, 2016.
- [25] Intel. Xetla- intel xe templates for linear algebra, <https://github.com/intel/xetla>.
- [26] Evangelos Georganas, Kunal Banerjee, Dhiraj Kalamkar, Sasikanth Avancha, Anand Venkat, Michael Anderson, Greg Henry, Hans Pabst, and Alexander Heinecke. Harnessing deep learning via a single building

- block. In *2020 IEEE International Parallel and Distributed Processing Symposium (IPDPS)*, pages 222–233. IEEE, 2020.
- [27] Ronan Keryell, Ruyman Reyes, and Lee Howes. Khronos sycl for opencl: a tutorial. In *Proceedings of the 3rd International Workshop on OpenCL*, pages 1–1, 2015.
 - [28] Samuel Williams, Andrew Waterman, and David Patterson. Roofline: an insightful visual performance model for multicore architectures. *Communications of the ACM*, 52(4):65–76, 2009.
 - [29] Falcon3-1b-instruct, <https://huggingface.co/tiiuae/Falcon3-1B-Instruct>.
 - [30] MobileLLM-paretoq-1.5b, <https://huggingface.co/facebook/MobileLLM-ParetoQ-1.5B-BF16>.
 - [31] Llama-3.1-8b, <https://huggingface.co/meta-llama/Llama-3.1-8B>.
 - [32] Evangelos Georganas, Dhiraj Kalamkar, Alexander Kozlov, and Alexander Heinecke. Ml-specqd: Multi-level speculative decoding with quantized drafts. *arXiv preprint arXiv:2503.13565*, 2025.

Optimization Notice: Software and workloads used in performance tests may have been optimized for performance only on Intel microprocessors. Performance tests, such as SYSmark and MobileMark, are measured using specific computer systems, components, software, operations and functions. Any change to any of those factors may cause the results to vary. You should consult other information and performance tests to assist you in fully evaluating your contemplated purchases, including the performance of that product when combined with other products. For more information go to <http://www.intel.com/performance>.

Intel, Xeon, and Intel Xeon Phi are trademarks of Intel Corporation in the U.S. and/or other countries.

APPENDIX

A. Reproducing end-to-end inference with PyTorch-TPP

To install the PyTorch-TPP runtime:

```
git clone https://github.com/libxsmm/
                                tpp-pytorch-extension.git
cd tpp-pytorch-extension
git checkout 2bit_gemm
git submodule update --init
bash utils/setup_conda.sh
source env.sh
python setup.py install
cd examples/llm/
pip install -r requirements.txt
```

In order to run the end-to-end inference experiments there is an exemplary script in `examples/llm:tpp_bakeoff_template.sh`. In this script one can define the number of P Cores (PCORES) and Total number of cores (CORES) (i.e. the number of E cores is CORES-PCORES).